cmgh
CELLULAR AND MOLECULAR GASTROENTEROLOGY AND HEPATOLOGY

ORIGINAL RESEARCH

Stratifin is Necessary for Spasmolytic Polypeptide-Expressing Metaplasia Development After Acute Gastric Injury

Yoonkyung Won,[1,2] Yoojin Sohn,[1,2,3] Su-Hyung Lee,[1,2,4] Anna Goldstein,[1,2] Rama Gangula,[5] Simon Mallal,[5] and James R. Goldenring[1,2,3,6]

[1]Section of Surgical Sciences, Vanderbilt University Medical Center, Nashville, Tennessee; [2]Epithelial Biology Center, Vanderbilt University Medical Center, Nashville, Tennessee; [3]Department of Cell and Developmental Biology, Vanderbilt University, Nashville, Tennessee; [4]Department of Veterinary Pathology, College of Veterinary Medicine, Konkuk University, Seoul, Republic of Korea; [5]Department of Medicine, Vanderbilt University Medical Center, Nashville, Tennessee; and [6]Nashville VA Medical Center, Nashville, Tennessee

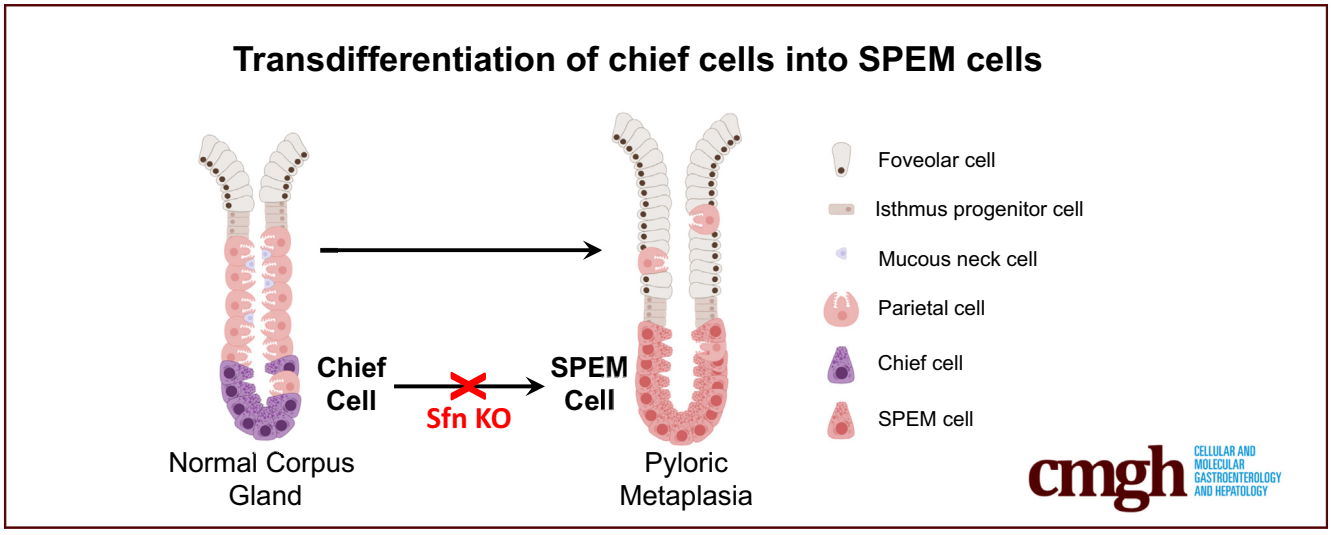

SUMMARY

Chief cells can transdifferentiate into spasmolytic polypeptide-expressing metaplasia after parietal cell loss in the stomach. We demonstrate that deletion of stratifin in chief cells impairs transdifferentiation of chief cells into spasmolytic polypeptide-expressing metaplasia after acute parietal cell loss.

BACKGROUND & AIMS: Chief cells can transdifferentiate into spasmolytic polypeptide-expressing metaplasia (SPEM), a metaplastic cell lineage, in response to acute injury after acid-secreting parietal cell loss in the stomach. Stratifin (SFN) acts as a multifunctional regulator, which can alter the function of multiple phosphoproteins. We have now examined how SFN contributes to the transdifferentiation of chief cells and the emergence of SPEM, as the initial metaplastic event in mucosal response to injury.

METHODS: We performed single-cell RNA sequencing on transdifferentiating chief cells after a single dose of DMP-777 treatment to induce acute parietal cell atrophy in *Mist1*^{CreERT2}; *LSL-tdTomato* mice. We generated a *Mist1*^{CreERT2}; *Sfn*$^{flox/flox}$ mouse model to examine the effects of SFN loss in the transdifferentiation of chief cells and SPEM development in response to acute injury. Histologic examination and immunostaining were performed in the mouse stomachs to assess cell lineage marker expression.

RESULTS: The single-cell RNA sequencing showed the initial characteristics of transdifferentiation of chief cells in response to acute injury. SFN expression was increased in transdifferentiating chief cells and SPEM cells. We determined that SFN loss in mice impairs the transdifferentiation of chief cells into SPEM following acute oxyntic atrophy in part by modulating EGFR/ERK signaling after acute injury.

CONCLUSIONS: SFN is essential for the initiation of reprogramming of chief cells during transdifferentiation and SPEM development. *(Cell Mol Gastroenterol Hepatol 2025;19:101521; https://doi.org/10.1016/j.jcmgh.2025.101521)*

Keywords: Gastric Chief Cells; Metaplasia; SPEM; Stratifin; Transdifferentiation; 14-3-3σ.

Gastric cancer is a leading cause of cancer-related mortality in the world. Cancer develops in the stomach in the setting of chronic atrophic gastritis usually in association with *Helicobacter pylori* infection.[1] Chronic injury associated with *H pylori* infection leads to prominent changes in the composition of the gastric mucosa, with loss of parietal cells, expansion of surface cells leading to foveolar hyperplasia, and the development of spasmolytic polypeptide-expressing metaplasia (SPEM), a cell lineage that resembles the basal mucous cells found in the deep antral glands.[2] Our group has demonstrated that SPEM arises from transdifferentiation of chief cells into mucous cell metaplasia in response to severe gastric injury in lineage mapping mouse models.[3,4] Because SPEM seems to be the initial metaplastic change in the face of oxyntic atrophy, it is crucial to understand how transdifferentiation of chief cells leads to the development of SPEM as a key initial event required for neoplastic transformation in the stomach.

The transdifferentiation of chief cells into SPEM occurs through an orderly program of changes in chief cells leading to lineage reprogramming,[3,5,6] including cessation of the zymogenic granule production accompanied by down-regulation of the transcription factor MIST1,[7] autophagic degradation of zymogen granules,[8] and up-regulation of the CD44v9-xCT pathway to deal with increased reactive oxygen species (ROS) together with mucous granule production.[9] However, although the SPEM lineage exhibits distinct molecular characteristics, the regulatory mechanisms involved in the transdifferentiation of chief cells into SPEM cells remain unclear.

Stratifin (SFN; 14-3-3σ) belongs to the 14-3-3 family of evolutionarily conserved proteins that are involved in the regulation of various cellular processes through the binding to phosphorylated proteins.[10] SFN functions as a multifaceted adapter protein that binds to partners through phosphoserine or phosphothreonine motifs and participates in a variety of cellular processes including signal transduction, cellular trafficking, cell proliferation, and differentiation.

In this study, we performed fluorescence-activated cell sorting (FACS) and single-cell RNA sequencing (scRNAseq) using *Mist1*^{CreERT2}; *LSL-tdTomato* mice to examine the initial transcriptional changes during the transdifferentiation of chief cells in response to oxyntic atrophy. We identified the up-regulation of SFN as an early step in the initiation of transdifferentiation of chief cells after acute gastric injury. We also examined the role of SFN in the transdifferentiation of chief cells toward SPEM development using the *Mist1*^{CreERT2}; *Sfn*$^{flox/flox}$ mouse model. In chief cell-directed *Sfn* knockout (KO) mice, SPEM development was impaired, and the chief cells did not reprogram into proliferative metaplastic cells after acute gastric injury. Our results suggest that loss of *Sfn* suppressed the development of SPEM after acute gastric injury.

Results

Gene Expression Profile of the Transdifferentiating Chief Cells in Response to Injury

To explore the earliest changes initiated in chief cells during transdifferentiation, we examined transcriptional changes in transdifferentiating chief cells using scRNAseq in *Mist1-CreERT2;LSL-tdTomato* (Mist1-tdTomato) mice. Tamoxifen was administered to mark Mist1+ chief cells with tdTomato expression, and 1 group of the mice were treated with a single dose of DMP-777 to chemically induce acute oxyntic atrophy. After 24 hours, we sorted the tdTomato-positive cells from untreated and DMP-777-treated corpus mucosa. Single cells were sorted into each well of 96-well microtiter plates containing barcodes for scRNAseq (Figure 1*A*).[11] The sequencing data were deconvolved and the gene expression patterns were analyzed by principal component analysis. Although only 155 FACS sorted cells were analyzed (65 from control animals and 90 from DMP-777-treated mice), these were sufficient to discern patterns among isolated populations. The principal component analysis plot showed that the tdTomato-positive cells from untreated mice and DMP-777-treated mice into distinct populations (Figure 1*B*). Previous studies demonstrated that the transdifferentiating chief cells expressed SPEM cell markers, including aquaporin 5 (*Aqp5)* and Trefoil Factor 2 (*Tff2),* together with zymogenic chief cell markers, including gastric intrinsic factor (*Gif*), pepsinogen C (*Pgc*), and *Rab3d*. The expression of *Pgc* and *Gif*, markers for gastric chief cells, was observed in untreated and DMP-777-treated populations of cells. In contrast, the expression of SPEM cell lineage markers, *Gkn3* and *Aqp5*, was up-regulated in DMP-777-treated cell populations (Figure 1*C*). The tdTomato-positive chief cells from DMP-777-treated stomach were enriched for SPEM cell lineage markers, including *Tff2*, *Gkn3*, *Aqp5*, *Wfdc2*, and *Sox9* and cell proliferation markers, *Mki67* and *Top2a*. However, the expression of gastric chief cell markers, such as *Pgc*, *Gif*, and *Rab3d* transcripts, was decreased compared with chief cells from the untreated stomach (Figure 1*D*), although the chief cell markers were still present in the tdTomato-positive chief cells from DMP-777-treated stomach (Figure 1*C*). Moreover, we found that *Mcm3*, *Mcm6*, and *Mcm7* proteins involved in chromatin unwinding, a process necessary for transcriptome alterations during the reprogramming of the chief cells,[12] were expressed in DMP-777-treated chief cells. These data suggest that tdTomato-positive cells from DMP-

Abbreviations used in this paper: **FACS, fluorescence-activated cell sorting; GSII, *Griffonia simplicifolia*; KO, knockout; PBS, phosphate-buffered saline; ROS, reactive oxygen species; scRNAseq, single-cell RNA sequencing; SFN, stratifin; SPEM, spasmolytic polypeptide-expressing metaplasia; WT, wild-type.**


Most current article

2352-345X
https://doi.org/10.1016/j.jcmgh.2025.101521

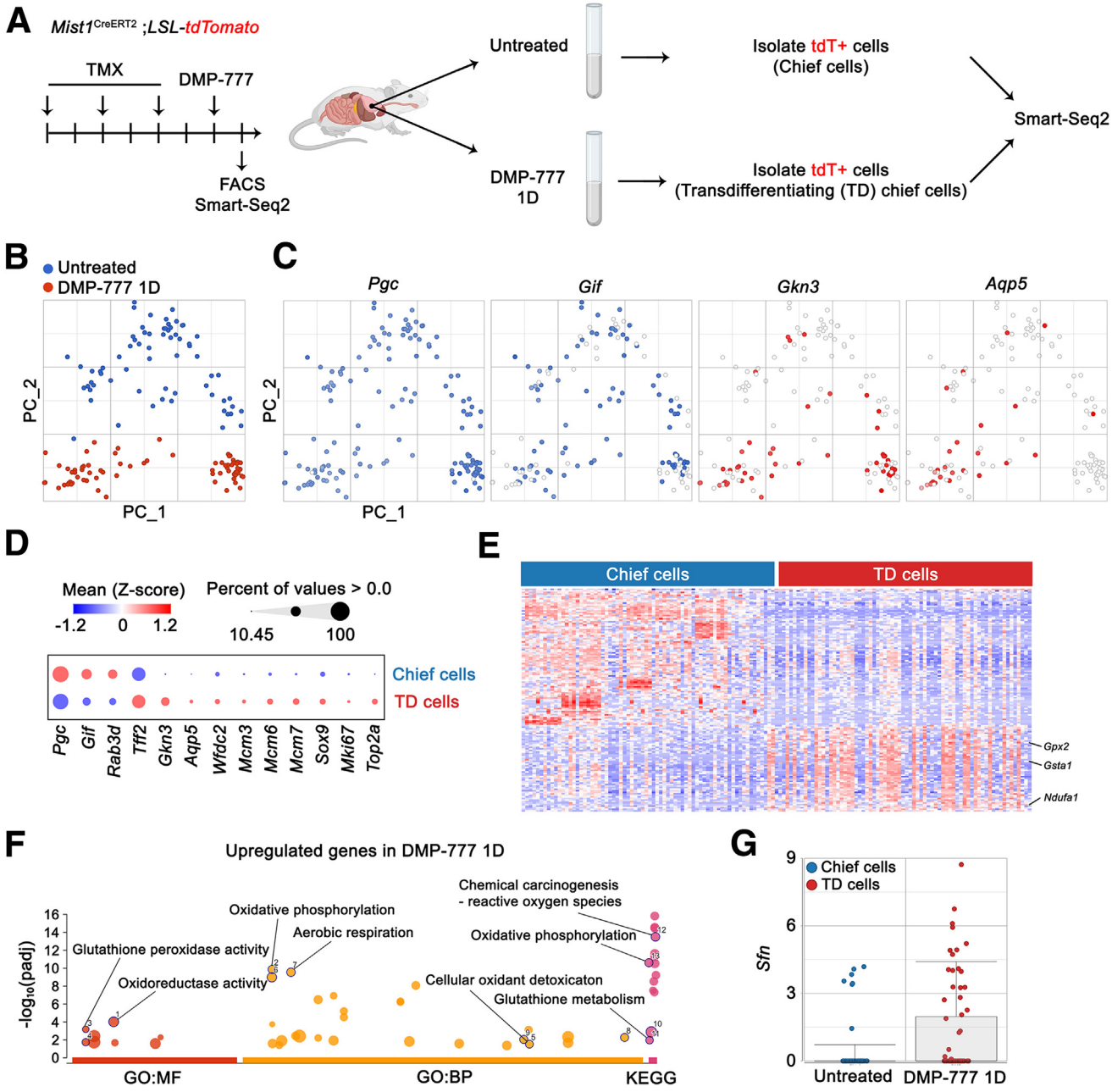

Figure 1. scRNAseq defines the transdifferentiation of chief cells in the corpus and their transcriptional changes after acute gastric injury. (*A*) Schematic of mouse experiments. (*B*) Principal component analysis (PCA) plot of untreated and DMP-777-treated condition. (*C*) PCA plots of chief cell markers (*Pgc* and *Gif*) and SPEM cell markers (*Gkn3* and *Aqp5*). (*D*) Bubble plot of chief cell markers (*Pgc*, *Gif*, and *Rab3d*), SPEM cell markers (*Tff2*, *Gkn3*, *Aqp5*, *Wfdc2*, *Mcm2*, *Mcm3*, *Mcm7*, and *Sox9*), and proliferating cell markers (*Mki67* and *Top2a*). (*E*) Heatmap of up-regulated and down-regulated genes in chief cells and transdifferentiating (TD) chief cells. (*F*) Functional enrichment analysis of top 100 up-regulated genes in TD chief cells. (*G*) Bar plot of normalized expression of Sfn in the untreated or 1 day of DMP-777-treated conditions.

777-treated stomach showed the transcriptional profiles of the transdifferentiating chief cells. To understand the detailed molecular characteristics of the transdifferentiating chief cells as the initial step in metaplasia development, we analyzed the bulk patterns of gene expression differences, and the pathways enriched in the populations of cells. We identified 661 differentially expressed genes that showed more than 2-fold (adjusted *P* value $< .01$) in DMP-777-treated stomach compared with untreated control. Functional enrichment analysis showed that the transdifferentiating chief cells were rapidly converted to an active metabolic state following gastric injury. The up-regulated genes in the transdifferentiating chief cells showed significant enrichment for ROS metabolism (*Gpx2*, *Gsta1*, and *Mgst3*) and oxidative phosphorylation (*Ndufa1*, *Ndufa4*, *Uqcr10*, *Uqcr11*, *Cox7a2*, *Cox7c*, and *Sdhd*) (Figure 1*E* and *F*). Previous studies have

shown that ROS detoxication and oxidative phosphorylation are involved in regulating cell fate in the transdifferentiation of chief cells after gastric injury.[9,13,14] These data suggest that chief cells undergo rapid transcriptional reprogramming to acquire the characteristics of SPEM cells after acute gastric injury.

SFN Expression is Up-regulated in Transdifferentiating Chief Cells and SPEM Cells After Acute Gastric Injury

We sought to identify potential early regulators involved in the transdifferentiation of chief cells into SPEM cell lineages from the scRNAseq data. We observed that *Sfn* expression was highly enriched in transdifferentiating chief cells in DMP-777-treated stomachs from the scRNAseq data (Figure 1*G*), as we previously observed in gastrin KO mice treated with DMP-777.[12] SFN, a 14-3-3 protein, is a multifunctional regulator that can alter the function and stability of multiple phosphoproteins.[15] We first validated the up-regulation of SFN in SPEM by examining the expression of SFN in conditionally immortalized cell lines derived from Immortomouse Chief (ImChief) and SPEM (ImSPEM) lineages.[16] *Sfn* mRNA expression showed a 15-fold increase in ImSPEM cells, and SFN protein was significantly increased in ImSPEM cells compared with ImChief cells (Figure 2*A* and *B*). Additionally, SFN expression was increased in mouse stomach tissues after L635 treatment, which, similar to DMP-777, induces acute oxyntic atrophy and SPEM development (Figure 2*C* and *D*).[3] To determine in which cells SFN expression increases, we performed immunostaining for SFN in stomach sections from wild-type (WT) mice treated with either L635 or DMP-777. The SFN protein was prominently expressed in the transdifferentiating chief cells that were copositive for CD44v9 or *Griffonia simplicifolia* (GSII)-lectin, SPEM cell lineage markers. In particular, SFN expression showed a marked increase starting from 5 days after DMP-777 treatment, with prominent staining of the basolateral membranes following acute gastric injury induced by either L635 or DMP-777 (Figure 2*E*-*G*). Furthermore, we also observed increased expression of SFN in stomachs from mice infected with *Helicobacter felis*, which causes chronic infection and inflammation in mice (Figure 2*H*). Lastly, we observed that SFN expression is up-regulated in human metaplastic cells, positive for CD44v9, at the base of glands (Figure 2*I*). These results indicate that SFN is up-regulated and localizes to the basolateral membrane in transdifferentiating chief cells and SPEM cells.

Loss of SFN Does Not Affect the Maintenance of Chief Cells

To determine the role of SFN in the process of chief cell transdifferentiation and SPEM development in vivo, we crossed the *Sfn* floxed allele mouse[17] with chief cell-specific *Mist1-CreERT2* mouse line (Figure 3*A*).[18,19] No histologic differences were observed between uninjured *Mist1*^{CreERT2}; *Sfn*$^{flox/flox}$ (Sfn KO) chief cells and WT chief cells (Figure 3*B*). The MIST1- and GIF-positive cells were maintained in Sfn KO chief cells compared with WT chief cells at the base of the glands (Figure 3*C*). Also, there was no significant difference between Sfn KO and WT mice in the number of MIST1-positive cells (Figure 3*D*).

SFN is Required for SPEM Development After Acute Gastric Injury

Next, we evaluated the impact of Sfn loss in chief cells on the induction of SPEM by acute oxyntic atrophy. We induced parietal cell loss and transdifferentiation of chief cells by L635 treatment in WT and Sfn KO mice (Figure 3*B*). We observed that Sfn KO did not affect parietal cell loss induced by L635 treatment by assessing parietal cell marker H^+K^+-ATPase expression, which showed no marked differences between WT and Sfn KO mice (Figure 3*E*). We next examined the expression of SFN in mouse stomach tissues after L635 treatment for 3 days. SFN expression was up-regulated in the L635-treated WT stomach. Notably, SFN expression was localized to the surface area of the stomach and was absent in the bases of corpus glands in Sfn KO mice (Figure 4*A* and *B*). Pyloric metaplasia induced by parietal cell loss in the corpus demonstrates SPEM cell lineages at the gland bases and the expansion of foveolar surface mucus cells.[2,4] These data suggest that most increased SFN expression was in SPEM cells, although some SFN expression was also observed in foveolar cells.

To determine if Sfn loss affects the development of SPEM cell lineages after acute gastric injury, we examined GSII-lectin-positive cells, which reflect mucus-secreting metaplastic cells. Although WT mice showed a prominent increase of GSII-lectin-positive cells at the base of the glands after L635 treatment, GSII-lectin-positive cells were not increased at the base of the glands in Sfn KO stomachs (Figure 4*A*). In WT mice, GSII-lectin expression was primarily localized to the base of the glands, whereas in Sfn KO mice, GSII-lectin-positive cells were distributed in the middle of the gland in a pattern characteristic of mucous neck cells in untreated stomachs (Figure 4*C*). These observations suggest Sfn deletion impairs the transdifferentiation of chief cells into SPEM cells.

SFN is Involved in Reprogramming into Proliferative SPEM Cells

Because continued injury and inflammation can promote the proliferation of metaplastic cells, we next investigated whether *Sfn* loss can affect the progression of SPEM into a more proliferative lineage. We performed immunostaining for the proliferation marker Ki-67 and the SPEM cell marker AQP5. AQP5 expression is up-regulated early in the process of transdifferentiation to SPEM.[20] In WT mice, SPEM cells entered a proliferative phase after 3 days of L635 treatment. In contrast, chief cells in Sfn KO mice did not enter the proliferative phase, although they showed an increase in

AQP5 expression (Figure 5*A*). In particular, Ki-67-positive cells were rarely observed at the base of glands in Sfn KO after 3 days of L635 treatment (Figure 5*B*). We also observed a notable decrease in the AQP5-positive cells at the base of the glands in Sfn KO mice compared with WT mice (Figure 5*C*). Together, these findings suggest that the loss of Sfn in chief cells impairs the progression to the proliferating SPEM cells.

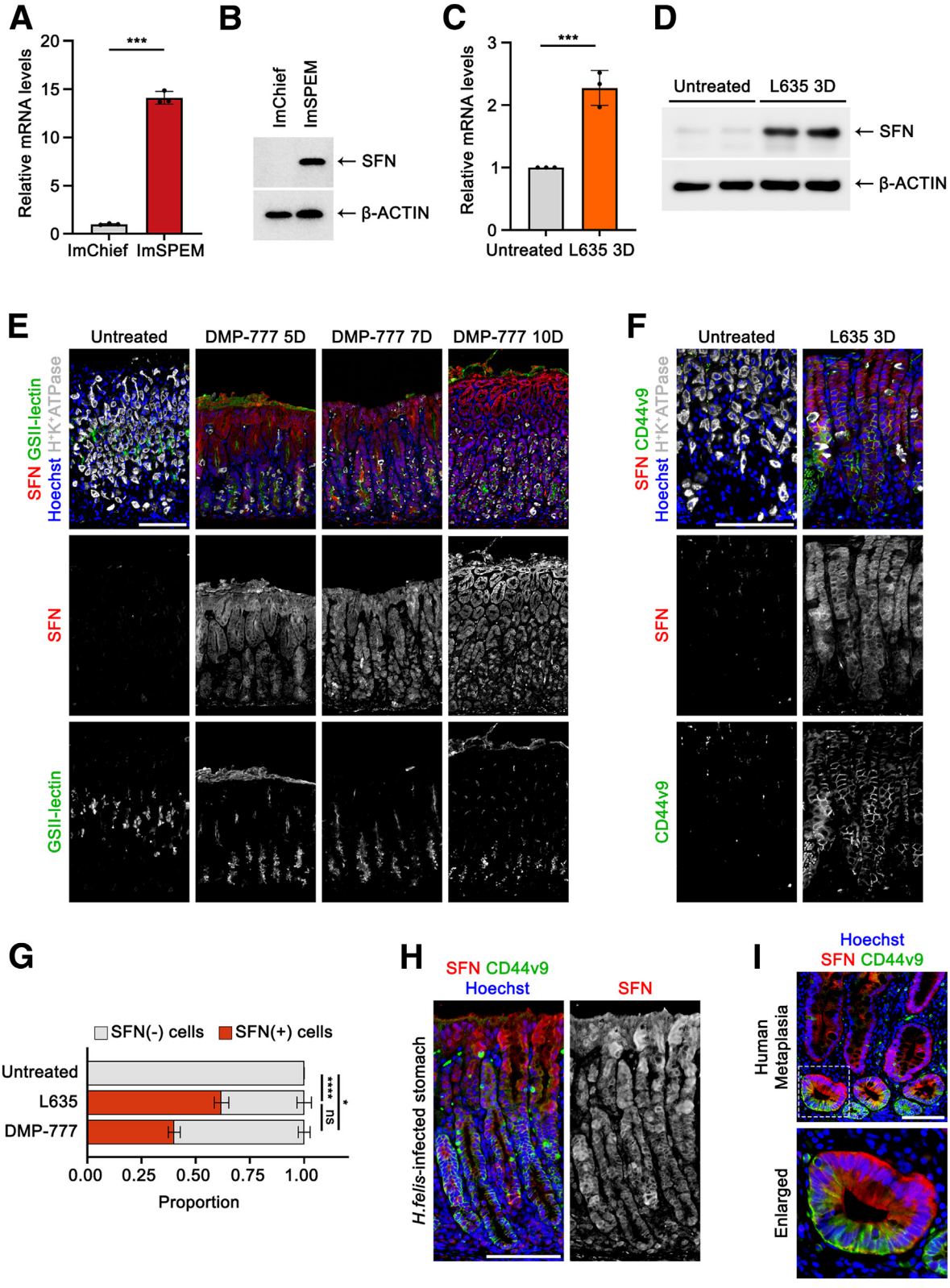

Loss of Sfn in Chief Cells Abolishes SOX9 Expression After Acute Gastric Injury

To further explore whether Sfn influences SPEM development through transcriptional changes during the early stages of the transdifferentiation of chief cells, we examined the expression of SOX9, a transcription factor critical for reprogramming chief cells into SPEM cells after acute gastric injury.[21] In stomachs from both WT and Sfn KO untreated mice, SOX9 was predominantly expressed in the neck and isthmic regions (Figure 6*A*). After 3 days of L635 treatment in WT mice, SOX9 expression was highly increased at the base of the glands, where SPEM cells are located. Additionally, MIST1 expression was down-regulated in both WT and Sfn KO mice after 3 days of L635 treatment. However, in Sfn KO mice, SOX9 up-regulation was barely observed after 3 days of L635 treatment (Figure 6*A* and *B*). To provide further clarification, we performed costaining for SFN and SOX9. In Sfn KO mice, SFN and SOX9 copositive cells were barely observed, whereas WT stomachs exhibited strong SOX9 expression with SFN copositivity (Figure 6*C*). These data suggest that Sfn regulates SOX9 expression, a transcription factor essential for SPEM development, to promote the transdifferentiation of chief cells into SPEM cells.

Loss of Sfn Affects EGFR Phosphorylation and ERK Signaling After Acute Gastric Injury

Previous reports have shown the participation of cellular signaling pathways including mTOR and receptor tyrosine kinase signaling pathways in the downstream response to oxyntic injury.[22–24] To determine if Sfn loss affects these cellular signaling pathways, we examined the activation of multiple cellular signaling pathways involved in SPEM development. Among the cellular signaling pathway markers, we observed that the EGFR and ERK phosphorylation were significantly increased in L635 treatment for 3 days in WT mice and decreased in Sfn KO mice after 3 days of L635 treatment (Figure 7*A-C*). However, other cell signaling pathways were not significantly affected by Sfn KO after 3 days of L635 treatment (Figure 7*A-C*). Moreover, we performed SOX9 and pEGFR costaining in L635-treated WT and Sfn KO stomach tissues to determine the spatial changes of EGFR phosphorylation. In WT mice, we observed strong up-regulation of SOX9 and pEGFR in cells at the base of glands where the SFN up-regulation occurs. Notably, the up-regulation was not evident in Sfn KO mice (Figure 7*D*). These data suggest that Sfn plays a role in regulating the activation of the EGFR/ERK signaling pathway.

Discussion

In this study, we focused on the functional roles of SFN in the transdifferentiation of chief cells and SPEM development after acute gastric injury. We have identified Sfn, also known as 14-3-3-sigma, as a candidate regulator of the transdifferentiation of chief cells and SPEM development, based on scRNAseq data of early transcriptional changes following acute gastric injury. Although the roles of SFN have been studied in many primary tumors and tumor cell lines including gastric cancer,[15,25] no previous studies have addressed SFN's function in metaplasia development. In this study, we investigated the role of SFN in initiation of the reprogramming of chief cells during transdifferentiation into SPEM cells by in vivo experiments using a chief cell-targeted Sfn KO mouse model. We also evaluated whether the loss of Sfn alters the orderly program of chief cell transdifferentiation. We demonstrated that SFN is responsible for the reprogramming of chief cells into SPEM cells after acute gastric injury in part via activation of the EGFR/ERK signaling pathway. A limitation of this study is that we have presently been unable to identify the intracellular phosphoproteins in chief cells that are targets for Sfn action. Because SFN expression is increased and relocalizes to the plasma membrane, we speculated that SFN is either binding newly phosphorylated targets or is promoting relocalization of phosphorylated targets to the plasma membrane. We have tried to find the binding partners of SFN using protein-proximity labeling and 3x-FLAG purification mass spectrometry. However, we have found that the binding between SFN and its binding proteins, particularly phosphorylated proteins, was unstable. When we tried to precipitate the binding proteins already implicated known as SFN binding proteins in BioGRID[26] databases, no specific proteins were identified. Thus, further experimentation is needed to define precisely SFN targets in transdifferentiating chief cells.

Transdifferentiation of chief cells requires a series of key transitions to down-regulate zymogen production, promote zymogen granule autophagy, provide protection against

Figure 2. (***See previous page***). **Up-regulation of Sfn in SPEM cell lineages.** (*A*) Quantitative polymerase chain reaction analysis of Sfn mRNA levels in ImChief cells (n = 3) and ImSPEM cells (n = 3). Two-tailed unpaired t-test. (*B*) Immunoblots for SFN or β-actin in ImChief cells (n = 3) and ImSPEM cells (n = 3). (*C*) Quantitative polymerase chain reaction analysis of Sfn mRNA levels in untreated (n = 3) and L635-treated mice (n = 3). Two-tailed unpaired t-test. (*D*) Immunoblots for SFN or β-actin in untreated (n = 2) and 3 days of L635-treated mice (n = 2). (*E*) Immunostained sections from WT untreated (n = 3), DMP-777-treated mice killed after 5 (n = 3), 7 (n = 3), or 10 (n = 4) days of DMP-777 treatment for SFN (*red*), SPEM cell marker GSII-lectin (*green*), and parietal cell marker H^+K^+ATPase (*white*), with nuclear counterstain Hoechst 33342 (*blue*). (*F*) Immunostained sections from WT untreated (n = 3), L635-treated (n = 4) mice killed after 3 days of L635 treatment for SFN (*red*), SPEM cell marker CD44v9 (*green*), and parietal cell marker H^+/K^+-ATPase (*white*), with nuclear counterstain Hoechst 33342 (*blue*). (*G*) Quantitation of positive cells for SFN. Data represent mean ± standard deviation (n = 9 images from 3 mice at 20x magnification in each group). Kruskal-Wallis test with 2-sided Dunn multiple comparison test. (*H*) Immunostained sections from *Helicobacter felis*–infected stomachs after 8 weeks postinfection (n = 3) for SFN (*red*) and SPEM cell marker CD44v9 (*green*) with nuclear counterstain Hoechst 33342 (*blue*). (*I*) Immunostained sections from human metaplastic regions for SFN (*red*) and SPEM cell marker CD44v9 (*green*) with nuclear counterstain Hoechst 33342 (*blue*). All panels show mean ± standard deviation. *$P < .05$, ***$P < .001$, ****$P < .0001$. ns, not significant. Scale bar = 100 μm.

ROS, and up-regulate production of mucin granules.[2,9,12,23] Our findings from scRNAseq revealed that up-regulation of Sfn is 1 of the early changes during the transdifferentiation of chief cells. Sfn was identified as a differentially expressed gene in our studies comparing SPEM cells and chief cells in humans and mice.[12,27,28] In this study, we demonstrated

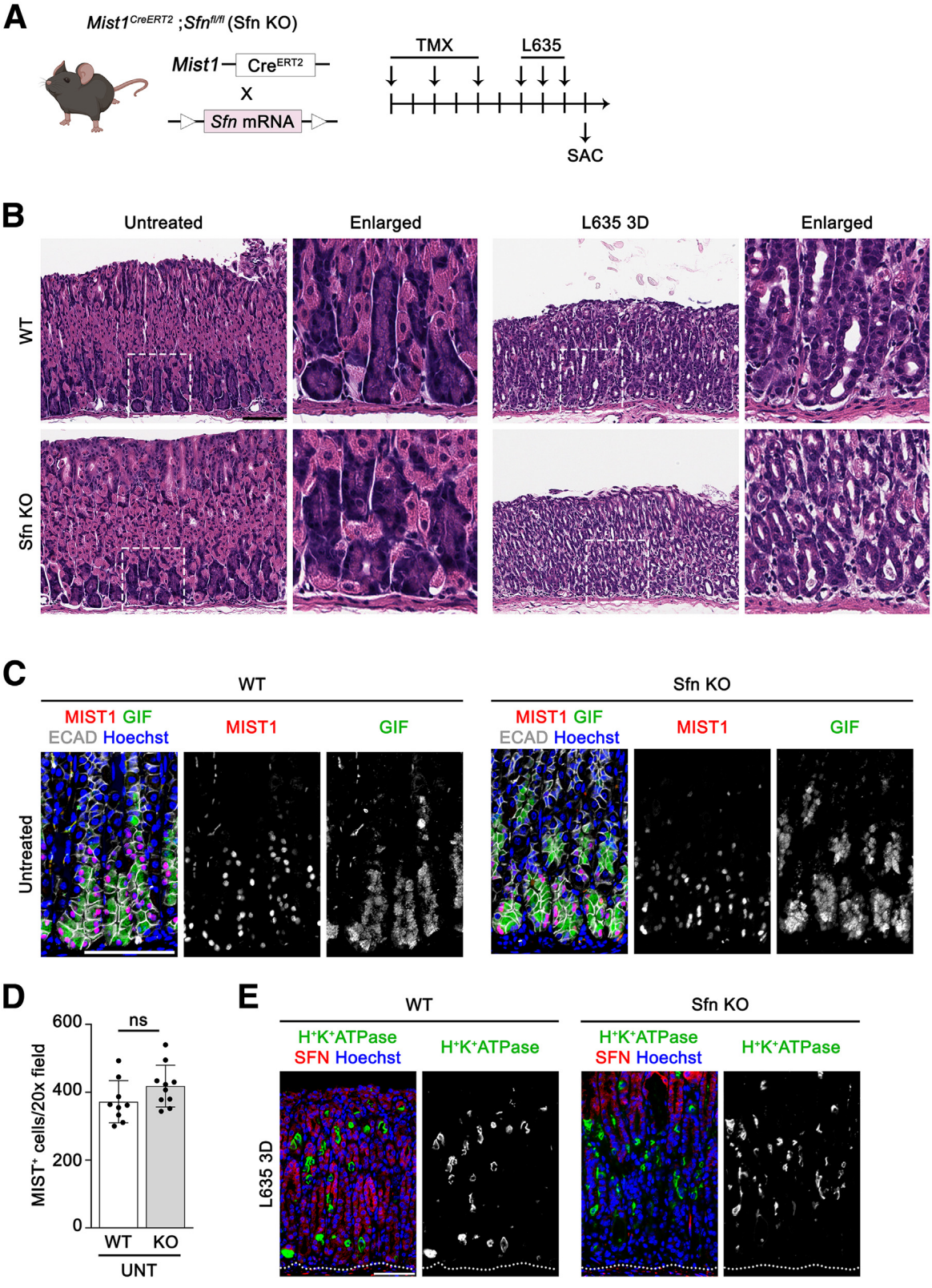

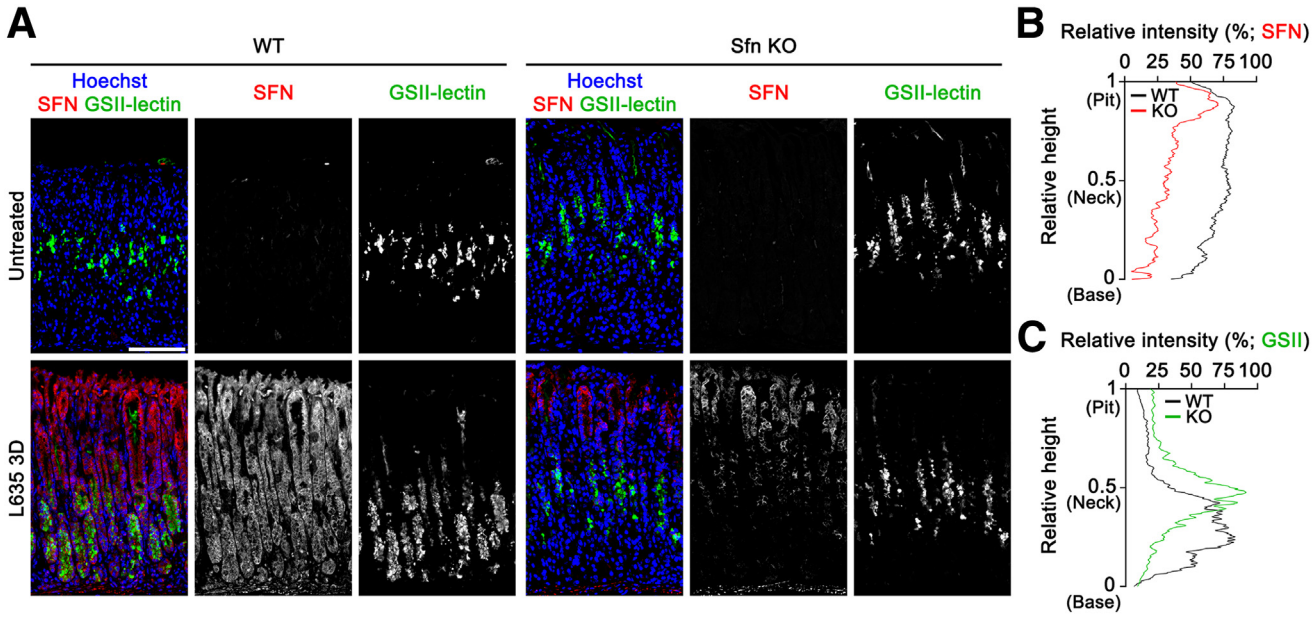

Figure 4. Sfn is indispensable for transdifferentiating chief cells into SPEM cells after acute gastric injury. (*A*) Immunostained sections from WT or Sfn KO mice for SFN (*red*) and SPEM cell marker GSII-lectin (*green*) with nuclear counterstain Hoechst 33342 (*blue*) in untreated or 3 days of L635 treatment. (*B*) Profiling of the expression of SFN across the corpus mucosal height (geometric mean value, n = 5 images from 3 mice per condition). (*C*) Profiling of the expression of GSII-lectin across the corpus mucosal height (geometric mean value, n = 5 images from 3 mice per condition).

that increased expression of Sfn in SPEM cells occurs early in the transdifferentiation process, but distal to the down-regulation of Mist1 and up-regulation of AQP5 in chief cells. This was evident in Sfn KO mice, where the loss of Sfn impaired the development of SPEM cells following acute gastric injury. Sfn KO mice also revealed significant disruption in the expression of key markers associated with SPEM. Notably, markers of the proliferative SPEM state, including Sox9 and Ki-67, were absent or significantly diminished in Sfn KO mice after injury. The inability of Sfn KO mice to up-regulate SOX9 after injury reinforces the idea that SFN is essential for initiating chief cell reprogramming. Furthermore, our signaling pathway studies suggest that SFN plays a crucial role in driving transdifferentiation toward a more proliferative and metaplastic state via such mechanisms as EGFR/ERK signaling.

Phosphorylation of AKT or STAT3 were not consistently increased in WT L635-treated stomachs, and Sfn KO stomachs did not show a significant decrease after 3 days of L635 treatment. Thus, these pathways may not strongly influence the initiation of transdifferentiation, and may rather contribute to later stages of carcinogenesis. Indeed, previous studies have noted that the PI3K/AKT/mTOR pathway plays a critical role in cell cycle regulation and promotes the development and metastasis of gastric cancer.[29,30] Also, the STAT3 pathway can contribute to tumorigenesis and drug resistance across various cancer cell types.[31] A recent study further suggested that the STAT3 pathway might be essential for the survival of dysplastic cells.[32] Thus, the EGFR/ERK signaling pathway seems to influence the development of metaplasia, which is the earliest step of gastric carcinogenesis.

In summary, our study highlights the critical role of SFN in the process of transdifferentiation and progression to SPEM cells. These findings provide new insights into the molecular mechanisms underlying metaplasia development and further demonstrate that the process of transdifferentiation proceeds through an orderly series of reprogramming events.

Materials and Methods

Mice

All mice used in this study followed protocols approved by the Institutional Animal Care and Use Committees of Vanderbilt University Medical Center. Littermates or age-matched mice were randomly allocated to experimental or control groups and equal numbers of male and female mice were used in all studies. The *Mist1*^{CreERT2}*; ROSA26-CAG-LoxP-*

Figure 3. (***See previous page***). **Sfn KO does not affect chief cell maintenance.** (*A*) Schematic for mouse experiments. L635 was administered to WT or Sfn KO mice for 3 days to induce acute gastric injury. (*B*) Hematoxylin and eosin–stained images from untreated or L635-treated stomach tissues in WT or Sfn KO mice. (*C*) Immunostained sections from WT untreated or Sfn KO untreated mice for chief cell marker MIST1 (*red*) and GIF (*green*), and epithelial membrane marker ECAD (*white*), with nuclear counterstain Hoechst 33342 (*blue*). (*D*) Quantitation of MIST1-positive cells per 20x field of images. Each *dot* indicates the MIST1-positive cells per x20 field of images. (*E*) Immunostained sections from WT or Sfn KO mice for SFN (*red*) and parietal cell marker H^+/K^+ATPase (*red*) with nuclear counterstain Hoechst 33342 (*blue*) after 3 days of L635 treatment. Scale bars: 100 μm (*B* and *C*). All panels show mean ± standard deviation. ns, not significant. n ≥ 3 mice per condition.

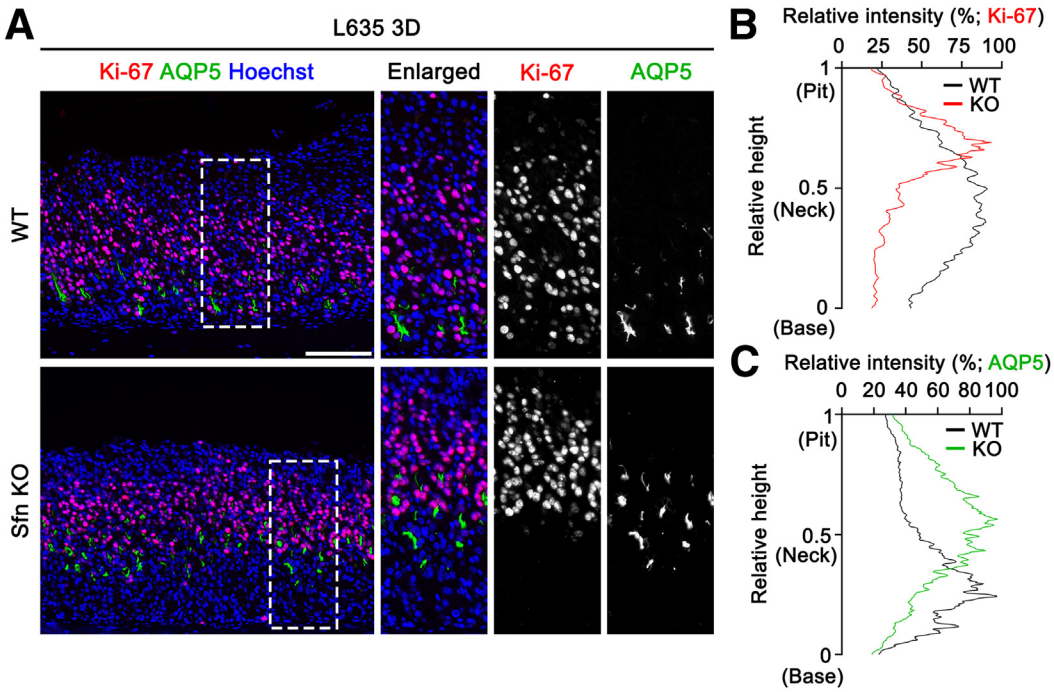

Figure 5. Sfn KO inhibits reprogramming into proliferative SPEM cells. (*A*) Immunostained sections from WT or Sfn KO mice for proliferation marker Ki-67 (*red*) and SPEM cell marker AQP5 (*green*) with nuclear counterstain Hoechst 33342 (*blue*) after 3 days of L635 treatment. (*B*) Profiling of the expression of Ki-67 across the corpus mucosal height (geometric mean value, n = 5 images from 3 mice per condition). (*C*) Profiling of the expression of AQP5 across the corpus mucosal height (geometric mean value, n = 5 images from 3 mice per condition).

Stop-LoxP (LSL)-tdTomato mice were used to compare the transcriptional changes between normal chief cells and transdifferentiating chief cells. The *Mist1*^{CreERT2} mice[19] were crossed with *ROSA26-CAG-LSL-tdTomato* mice (Strain no. 007914, Jackson Laboratories, Bar Harbor, ME). We also crossed *Mist1*^{CreERT2} with *Sfn*$^{flox/flox}$ mice (*Mist1*^{CreERT2};*Sfn*$^{flox/flox}$ *mice)* to examine the function of Sfn. The *Sfn*$^{flox/flox}$ mouse strain was obtained from the European Mouse Mutant Archive repository (EM:02444). At 6–8 weeks of age, the mice were treated with tamoxifen by subcutaneous injections 3 times every other day (5 mg in corn oil; T5648 and C8267, Sigma). At 2 days after the end of the last tamoxifen treatment, the mice were treated with L635 once a day for 3 doses by oral gavage (Chemical Synthesis Core of the Vanderbilt Institute of Chemical Biology; 350 mg/kg) or DMP-777 (350 mg/kg) once a day for 1, 3, 5, and 10 days. Details for the experimental scheme are described in Figure 1*A* and Figure 3*A*.

Helicobacter felis *Infection*

Six- to 8-week-old WT C57BL/6 were purchased from The Jackson Laboratory. *H felis* was cultured on *Brucella* broth containing 10% fetal bovine serum at 37°C under a microaerobic condition using a GasPak EZ Campy Container System (BD Biosciences, San Jose, CA). At 8 weeks of age, the mice were fasted for 12 hours and infected with 200 μL of *H felis* (5×10^8 colony-forming units/mL) by oral gavage 4 times at 2-day intervals. The stomach was harvested 8 weeks after infection and fixed in 10% neutral-buffered formalin for histopathologic analysis.

Gastric Gland Single Cell Isolation

Mouse stomachs were harvested, opened along the greater curvature, and washed in ice-cold phosphate-buffered saline (PBS) without Ca^{2+} and Mg^{2+}. The antrum was removed with a razor blade and the oxyntic mucosa was harvested with a cell scraper to separate the mucosa from the serosa. The corpus mucosa was finely minced using a razor blade and digested in digestion buffer (Advanced DMEM/F12 + 5% fetal bovine serum + 1 mg/mL collagenase type 1a + DNase I) at 37°C with shaking at 220 rpm for 30 minutes. To stop the reaction, Advanced DMEM/F12 supplemented with 10 μM Y-27632 and 1 mM DTT was added. The mixture was centrifuged at 300 *g* for 5 minutes to pellet glands/cells. The supernatant was aspirated, and glands/cells were resuspended in TrypLE Express supplemented with 10 μM Y-27632 and incubated at 37°C for 7 minutes. Advanced DMEM/F12 supplemented with 10 μM Y-27632 was added to the TrypLE Express solution and centrifuged at 300 *g* for 5 minutes. The supernatant was removed, and cells were resuspended in 1 mL of Advanced DMEM/F12 + 1% fetal bovine serum + DNase I supplemented with 10 μM Y-27632 and stored on ice.

Fluorescence-Activated Cell Sorting and Single-Cell RNA Sequencing

For FACS, cells were resuspended in FACS buffer (1X PBS + 3% fetal bovine serum) and incubated with 1.0 mg/mL DAPI to exclude dead cells based on DAPI staining. Using a BD FACS Aria III (BD Biosciences), individual tdTomato-positive chief cells were sorted into 96-well plates

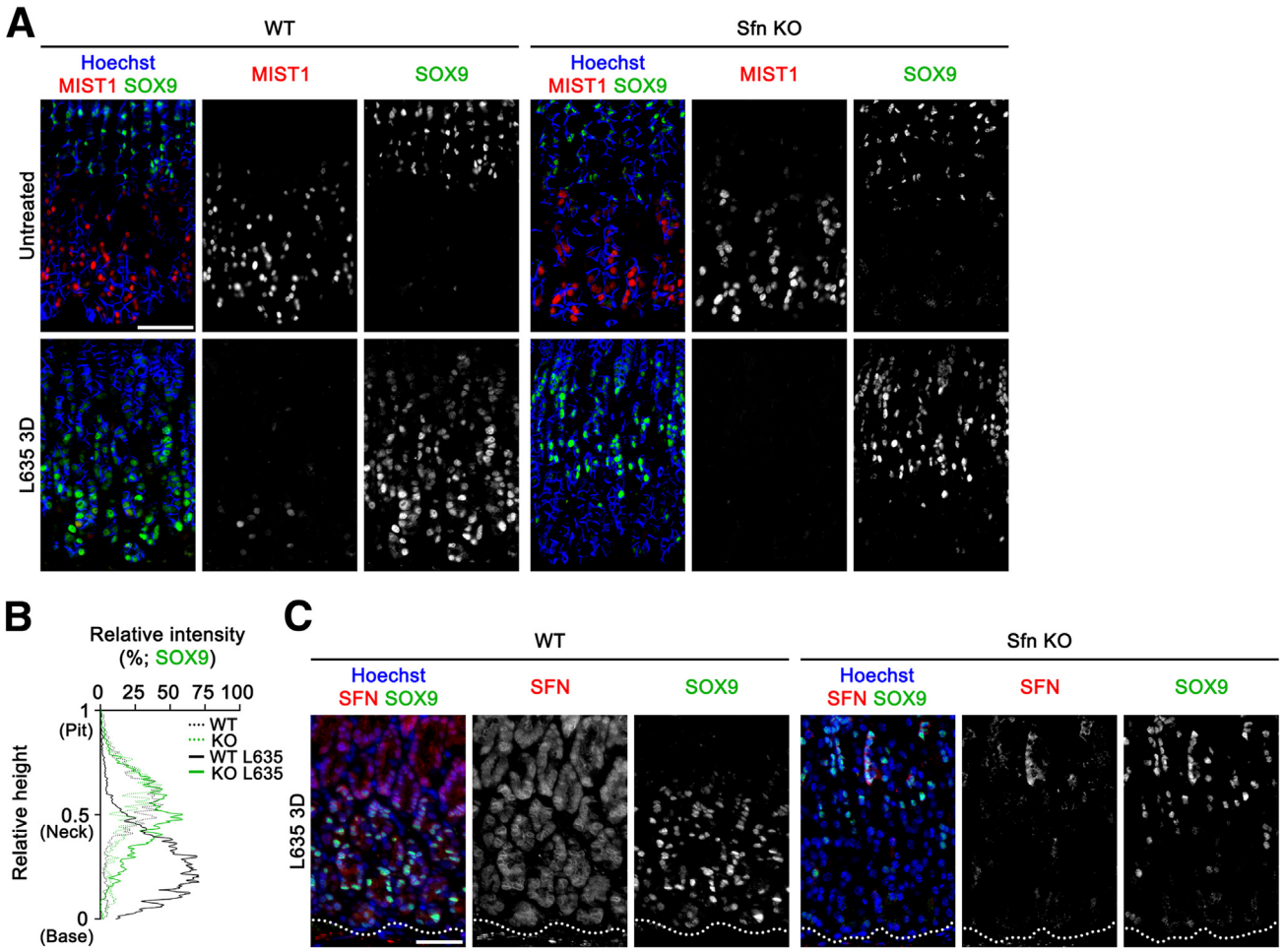

Figure 6. SOX9 expression does not increase in Sfn KO. (*A*) Immunostained sections from WT or Sfn KO mice for chief cell marker MIST1 (*red*), SPEM cell marker SOX9, and epithelial cell membrane marker ECAD (*blue*) in untreated or 3 days of L635 treatment. (*B*) Profiling of the expression of SOX9 across the corpus mucosal height (geometric mean value, n = 6 images from 3 mice per condition). (*C*) Immunostained sections from WT or Sfn KO mice for SFN (*red*) and SPEM cell marker SOX9 (*green*) with nuclear counterstain Hoechst 33342 (*blue*) after 3 days of L635 treatment. n ≥ 3 mice per condition.

containing lysis buffer and barcoded primers. scRNAseq was then performed as previously described using the Smart-seq2 method.[11,33] Sequencing of the cDNA libraries was performed on an Illumina NovaSeq 6000 instrument at the Vanderbilt Technologies for Advanced Genomics core facility, with a minimum sequencing depth of 100,000,000 reads per sample. Sequencing reads were trimmed and aligned by STAR (2.7.3a) with reference mouse genome, mm10. Gene expression profiles of 165 cells (75 cells from untreated mice and 90 cells from DMP-777-treated mice) were retrieved corresponding to high-quality cells. The sequencing data were analyzed using the PartekFlow (Partek). Cells from the tdTomato-positive cells from untreated mice or DMP-777-treated mice were clustered using principal component analysis. Each cluster of cells was annotated by the expression of known marker genes of gastric chief cells and metaplastic cells.[12,16] Functional enrichment analysis of differentially expressed genes filtered with adjusted *P* value < .01 and fold change >2 was implemented and analyzed using Web-based gProfiler.[34]

Histology and Immunostaining

Before paraffin embedding, mouse stomach tissues were isolated and fixed overnight in 4% paraformaldehyde. Paraffin-embedded tissues were sectioned at a thickness of 5 μm and stained with hematoxylin and eosin. For immunostaining, unstained paraffin sections were deparaffinized in HistoClear (HS-200, National Diagnostics) and rehydrated through serial dilutions of ethanol. Antigen retrieval was performed in a target retrieval solution (S1699, Agilent) using a pressure cooker for 15 minutes. Sections were rinsed in distilled water and incubated with Serum-free Protein Block Solution (X0909, Agilent) for 1.5 hours at room temperature. Sections were additionally incubated with Mouse-on-Mouse Blocking Reagent (MKB-2213-1, Vector Laboratories) for 30 minutes at room temperature to block nonspecific mouse antigens on mouse tissues. Primary antibodies (Supplementary Table 1) were diluted in Antibody Diluent (S3022, Agilent) and applied to sections overnight at 4°C in a humidified chamber.

For immunofluorescence, sections were washed with 1X PBS and incubated with Alexa-conjugated secondary

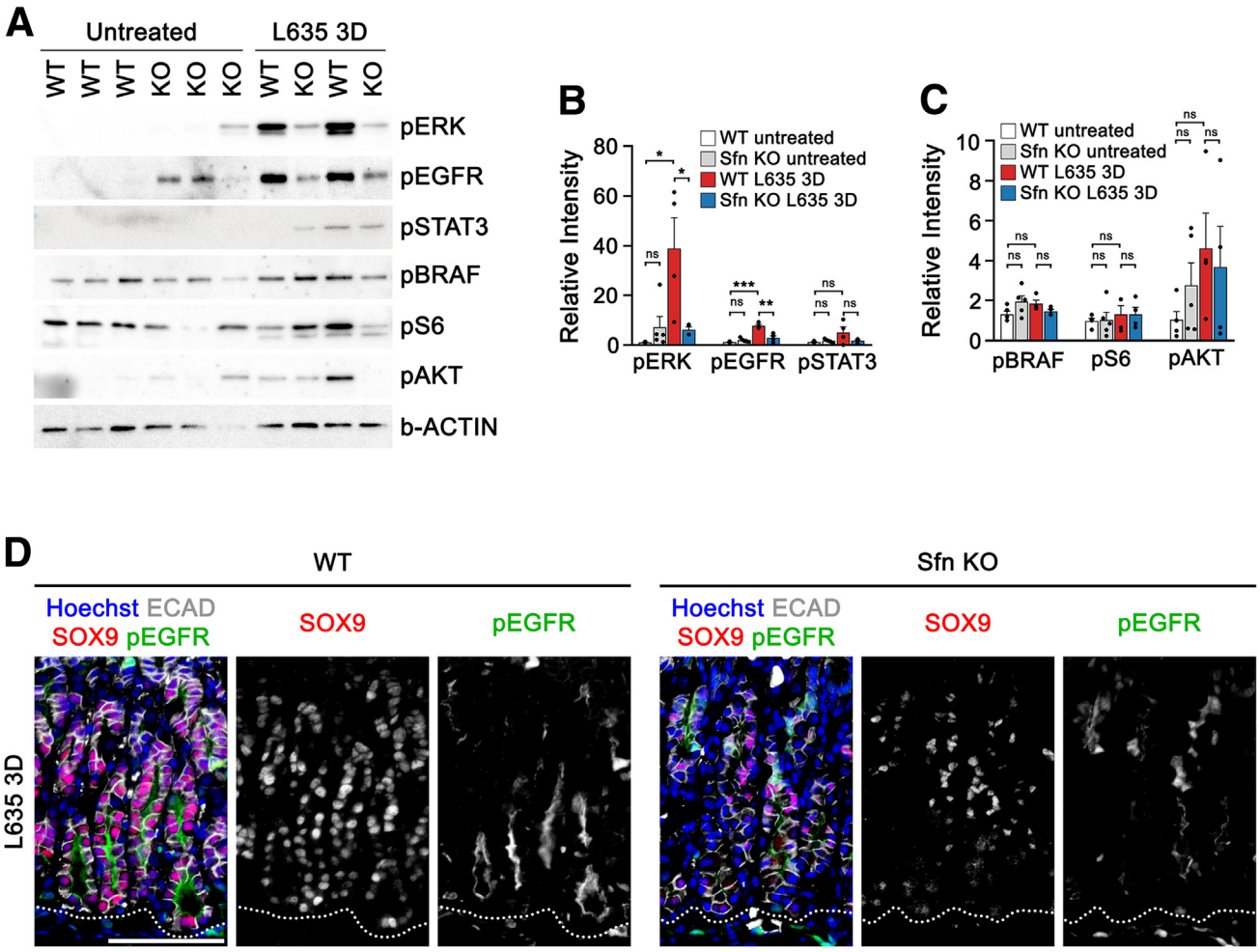

Figure 7. The EGFR/ERK signaling pathway is regulated by Sfn. (*A*) Immunoblots for phosphorylated ERK (pERK), tyrosine 1068-phosphorylated EGFR (pEGFR), tyrosine 705-phosphorylated STAT3 (pSTAT3), serine 729-phosphorylated BRAF (pBRAF), serine 240/244-phosphorylated S6 (pS6), serine 473-phosphorylated AKT (pAKT), or β-actin (b-actin) loading control for corpus mucosal tissues. (*B, C*) Quantitation of immunoblots for phosphorylated proteins in WT untreated (n = 5), Sfn KO untreated (n = 5), WT mice sacrificed after 3 days of L635 treatment (n = 4), and Sfn KO mice sacrificed after 3 days of L635 treatment (n = 4). All panels show mean ± standard deviation. *$P < .05$, ***$P < .001$. ns, not significant. (*D*) Immunostained sections from WT or Sfn KO mice for SPEM cell marker SOX9 (*red*), phosphorylated EGFR (*green*), and E-cadherin (ECAD, *grayscale*) with nuclear counterstain Hoechst 33342 (*blue*) after 3 days of L635 treatment. Scale bar = 100 μm.

antibodies (Life Technologies, 1:500) for 1 hour at room temperature. Sections were washed with 1X PBS and incubated with Hoechst 33342 (62249, Thermo Fisher Scientific, 1:5000) for 5 minutes at room temperature.

Image Analysis and Quantitation

All the images were captured on a Zeiss Axio Imager M2 microscope using an Axiovision digital imaging system at x20 magnification. The positivity of each cell lineage marker was manually quantitated using ZEN 3.2 software. Profiling of SFN, GSII-lectin, Ki-67, or AQP5 intensities, along with the height of each mouse corpus mucosa in 5 images from n = 3 mice per group, was automatically performed with ZEN 3.2 software.

RNA Extraction and Quantitative Polymerase Chain Reaction

Total RNA was extracted from mouse gastric organoids using the TRIzol Reagent (15596026, Thermo Fisher Scientific) following the manufacturer's protocol. cDNA was synthesized from 1 μg of RNA using the iScript gDNA Clear cDNA Synthesis Kit (1725035, Bio-Rad). Quantitative polymerase chain reaction was performed using the iTaq Universal SYBR Green Supermix (1725121, Bio-Rad) following the manufacturer's protocol on a Biorad CFX96 Real-Time PCR Detection System. *Actb* was used for the normalization of gene expression level and $2^{-\Delta\Delta Ct}$ method was used for relative quantification. Primer sequences used for quantitative polymerase chain reaction are listed in Supplementary Table 2.

Western Blot and Quantification

Total cell lysates were prepared using RIPA lysis buffer (R0278; Sigma). All lysis buffers contained protease inhibitors (P8340; Sigma) and phosphatase inhibitors (P5726 and P0044; Sigma). The proteins were fractionated by sodium dodecyl sulfate–polyacrylamide gel electrophoresis and transferred to a PVDF membrane. Antibodies used for Western blot are listed in Supplementary Table 1. Quantitation of immunoblots was performed using ImageJ analysis software. The integrated densities of target proteins were divided by integrated densities of loading control (b-actin) and normalized to the mean value of the WT untreated group.

Software

Graphics were generated in BioRender (https://biorender.com).

Statistical Analysis

Statistical analysis was performed using GraphPad Prism 9 (GraphPad Software, Inc). Normality testing (Shapiro-Wilk test) was conducted to determine whether to use parametric or nonparametric statistical tests. For 2 group comparisons, normally distributed data were analyzed by 2-tailed unpaired Student t test (equal standard deviation) or Welch t test (unequal standard deviation), whereas nonnormally distributed data were analyzed by Mann-Whitney test. Every experiment was repeated at least 3 times. The number of independent replicates of experiments, variation (mean ± standard deviation), and statistical test (P value) are described in the figure legends. Significance levels are indicated as $^{*}P < .05$, $^{**}P < .01$, or $^{***}P < .001$.

Supplementary Material

Note: To access the supplementary material accompanying this article, visit the full text version at https://doi.org/10.1016/j.jcmgh.2025.101521.

References

1. Zhang ZF, Kurtz RC, Klimstra DS, et al. *Helicobacter pylori* infection on the risk of stomach cancer and chronic atrophic gastritis. Cancer Detect Prev 1999;23:357–367.
2. Goldenring JR, Mills JC. Cellular plasticity, reprogramming, and regeneration: metaplasia in the stomach and beyond. Gastroenterology 2022;162:415–430.
3. Nam KT, Lee HJ, Sousa JF, et al. Mature chief cells are cryptic progenitors for metaplasia in the stomach. Gastroenterology 2010;139:2028–2037.e9.
4. Caldwell B, Meyer AR, Weis JA, et al. Chief cell plasticity is the origin of metaplasia following acute injury in the stomach mucosa. Gut 2022;71:1068–1077.
5. Mills JC, Goldenring JR. Metaplasia in the stomach arises from gastric chief cells. Cell Mol Gastroenterol Hepatol 2017;4:85–88.
6. Mills JC, Sansom OJ. Reserve stem cells: differentiated cells reprogram to fuel repair, metaplasia, and neoplasia in the adult gastrointestinal tract. Sci Signal 2015;8:re8.
7. Lennerz JK, Kim SH, Oates EL, et al. The transcription factor MIST1 is a novel human gastric chief cell marker whose expression is lost in metaplasia, dysplasia, and carcinoma. Am J Pathol 2010;177:1514–1533.
8. Radyk MD, Spatz LB, Pena BL, et al. ATF3 induces RAB7 to govern autodegradation in paligenosis, a conserved cell plasticity program. EMBO Rep 2021;22:e51806.
9. Meyer AR, Engevik AC, Willet SG, et al. Cystine/glutamate antiporter (xCT) is required for chief cell plasticity after gastric injury. Cell Mol Gastroenterol Hepatol 2019;8:379–405.
10. Pennington KL, Chan TY, Torres MP, et al. The dynamic and stress-adaptive signaling hub of 14-3-3: emerging mechanisms of regulation and context-dependent protein-protein interactions. Oncogene 2018;37:5587–5604.
11. Meyer AR, Engevik AC, Madorsky T, et al. Group 2 innate lymphoid cells coordinate damage response in the stomach. Gastroenterology 2020;159:2077–2091.e8.
12. Nozaki K, Ogawa M, Williams JA, et al. A molecular signature of gastric metaplasia arising in response to acute parietal cell loss. Gastroenterology 2008;134:511–521.
13. Miao ZF, Sun JX, Huang XZ, et al. Metaplastic regeneration in the mouse stomach requires a reactive oxygen species pathway. Dev Cell 2024;59:1175–1191.e7.
14. Chakrabarty RP, Chandel NS. Mitochondria as signaling organelles control mammalian stem cell fate. Cell Stem Cell 2021;28:394–408.
15. Shiba-Ishii A, Kano J, Morishita Y, et al. High expression of stratifin is a universal abnormality during the course of malignant progression of early-stage lung adenocarcinoma. Int J Cancer 2011;129:2445–2453.
16. Weis VG, Petersen CP, Mills JC, et al. Establishment of novel in vitro mouse chief cell and SPEM cultures identifies MAL2 as a marker of metaplasia in the stomach. Am J Physiol Gastrointest Liver Physiol 2014;307:G777–G792.
17. Winter M, Lodygin D, Verdoodt B, et al. Deletion of 14-3-3sigma sensitizes mice to DMBA/TPA-induced papillomatosis. Oncotarget 2016;7:46862–46870.
18. Shi G, Zhu L, Sun Y, et al. Loss of the acinar-restricted transcription factor Mist1 accelerates Kras-induced pancreatic intraepithelial neoplasia. Gastroenterology 2009;136:1368–1378.
19. Choi E, Hendley AM, Bailey JM, et al. Expression of activated ras in gastric chief cells of mice leads to the full spectrum of metaplastic lineage transitions. Gastroenterology 2016;150:918–930.e13.
20. Lee SH, Jang B, Min J, et al. Up-regulation of aquaporin 5 defines spasmolytic polypeptide-expressing metaplasia and progression to incomplete intestinal metaplasia. Cell Mol Gastroenterol Hepatol 2022;13:199–217.
21. Willet SG, Thanintorn N, McNeill H, et al. SOX9 governs gastric mucous neck cell identity and is required for injury-induced metaplasia. Cell Mol Gastroenterol Hepatol 2023;16:325–339.

22. Willet SG, Lewis MA, Miao ZF, et al. Regenerative proliferation of differentiated cells by mTORC1-dependent paligenosis. EMBO J 2018;37:e98311.
23. Miao ZF, Lewis MA, Cho CJ, et al. A dedicated evolutionarily conserved molecular network licenses differentiated cells to return to the cell cycle. Dev Cell 2020; 55:178–194.e7.
24. Lee SH, Won Y, Gibbs D, et al. Amphiregulin switches progenitor cell fate for lineage commitment during gastric mucosal regeneration. Gastroenterology 2024; 167:469–484.
25. Zhou WH, Tang F, Xu J, et al. Aberrant upregulation of 14-3-3o expression serves as an inferior prognostic biomarker for gastric cancer. BMC Cancer 2011; 11:397.
26. Chatr-Aryamontri A, Oughtred R, Boucher L, et al. The BioGRID interaction database: 2017 update. Nucleic Acids Res 2017;45:D369–D379.
27. Lee HJ, Nam KT, Park HS, et al. Gene expression profiling of metaplastic lineages identifies CDH17 as a prognostic marker in early stage gastric cancer. Gastroenterology 2010;139:213–225.e3.
28. Weis VG, Sousa JF, LaFleur BJ, et al. Heterogeneity in mouse spasmolytic polypeptide-expressing metaplasia lineages identifies markers of metaplastic progression. Gut 2013;62:1270–1279.
29. Liu L, Ye Y, Zhu X. MMP-9 secreted by tumor associated macrophages promoted gastric cancer metastasis through a PI3K/AKT/Snail pathway. Biomed Pharmacother 2019;117:109096.
30. Rong L, Li Z, Leng X, et al. Salidroside induces apoptosis and protective autophagy in human gastric cancer AGS cells through the PI3K/Akt/mTOR pathway. Biomed Pharmacother 2020;122:109726.
31. Lee HJ, Zhuang G, Cao Y, et al. Drug resistance via feedback activation of Stat3 in oncogene-addicted cancer cells. Cancer Cell 2014;26:207–221.
32. Kim H, Jang B, Zhang C, et al. Targeting stem cells and dysplastic features with dual MEK/ERK and STAT3 suppression in gastric carcinogenesis. Gastroenterology 2024;166:117–131.
33. Picelli S, Faridani OR, Bjorklund AK, et al. Full-length RNA-seq from single cells using Smart-seq2. Nat Protoc 2014;9:171–181.
34. Kolberg L, Raudvere U, Kuzmin I, et al. g:Profiler-interoperable web service for functional enrichment analysis and gene identifier mapping (2023 update). Nucleic Acids Res 2023;51:W207–W212.

Received October 28, 2024. Accepted April 16, 2025.

Correspondence
Address correspondence to: James R. Goldenring, MD, PhD, AGAF, Epithelial Biology Center, Vanderbilt University Medical Center, MRB IV 10435G, 2213 Garland Avenue, Nashville, Tennessee 37232-2733. e-mail: jim.goldenring@vumc.org.

Acknowledgments
Yoonkyung Won and Yoojin Sohn contributed equally to this work.

CRediT Authorship Contributions

Yoonkyung Won, PhD (Conceptualization: Equal; Data curation: Equal; Formal analysis: Equal; Investigation: Equal; Methodology: Equal; Validation: Equal; Visualization: Equal; Writing – original draft: Lead)

Yoojin Sohn (Conceptualization: Equal; Data curation: Equal; Formal analysis: Equal; Investigation: Equal; Methodology: Equal; Resources: Equal; Validation: Equal; Visualization: Equal; Writing – original draft: Equal)

Su-Hyung Lee, DVM, PhD (Data curation: Supporting; Investigation: Supporting; Methodology: Supporting; Supervision: Supporting; Writing – review & editing: Supporting)

Anna Goldstein (Investigation: Supporting; Methodology: Supporting; Writing – review & editing: Supporting)

Rama Gangula (Data curation: Supporting; Formal analysis: Supporting; Methodology: Supporting; Writing – review & editing: Supporting)

Simon Mallal (Resources: Supporting; Supervision: Supporting; Writing – review & editing: Supporting)

James R. Goldenring, MD, PhD (Conceptualization: Equal; Funding acquisition: Lead; Investigation: Equal; Methodology: Supporting; Project administration: Lead; Resources: Supporting; Supervision: Supporting; Visualization: Supporting; Writing – review & editing: Supporting)

Conflicts of interest
The authors disclose no conflicts.

Funding
This work was supported by grants from a Department of Veterans Affairs Merit Review Award IBX000930, Department of Defense CA190172, and National Institutes of Health R01 DK101332 and R01 CA272687 (to James R. Goldenring). This work was supported by the National Research Foundation of Korea grant funded by the Korean government (No. 2019R1A5A2027521). Core Services were performed through Vanderbilt University Medical Center's Digestive Disease Research Center (P30 DK058404) and Vanderbilt Ingram Cancer Center (P30 CA068485) with imaging in the Vanderbilt Digital Histology Shared supported by a VA Shared Instrumentation grant (1IS1BX003097).